

# Workflow assessing the effect of Achilles tendon rupture on gait function and metatarsal stress: Combined musculoskeletal modeling and finite element analysis

Dong Sun<sup>1</sup>, Yang Song<sup>1,2,3</sup>, Xuanzhen Cen<sup>1,2,3</sup>, Meizi Wang<sup>1,2</sup>, Julien Steven Baker<sup>4</sup> and Yaodong Gu<sup>1</sup> 

## Abstract

Achilles tendon rupture (ATR) incidence has increased among badminton players in recent years. The foot internal stress was hard to obtain through experimental testing. The purpose of the current research is to develop a methodology that could improve the finite element model derived foot internal stress prediction for ATR clinical and rehabilitation applications. A subject-specific musculoskeletal model was combined with a 3D finite element model to predict the metatarsal stress. The 80% point during the push-off phase of walking was selected for the comparing between injured and uninjured sides. The surgical repaired Achilles tendon (AT) after 12 months was elongated by 5.5% than the uninjured tendon. At 80% point of stance phase, the ankle plantarflexion angle and AT force decreased by 39.6% and 21.9% on the injured side, respectively. The foot inversion degree increased by 22.9% and was accompanied by the redistribution of metatarsals von Mises stress. The stresses on the fourth and fifth metatarsals were increased by 59.5% and 85.9% on the injured side. The workflow is available to assess musculoskeletal disorders and obtain foot internal stress after ATR. The decreased ankle plantar flexor force may be affected by triceps surae muscle atrophy and weakened force transmission ability of elongated AT. The increased von Mises stress on fourth and fifth metatarsals accompanied by higher foot inversion may increase the ankle lateral sprain injury risk.

## Keywords

Achilles tendon rupture, musculoskeletal model, finite element model, gait analysis, metatarsal stress

Date received: 1 October 2021; accepted: 17 February 2022

## Introduction

The Achilles tendon (AT) is the largest and thickest tendon structure in the body, consisting of the calf triceps tendon (which includes the medial and lateral gastrocnemius and the soleus muscle).<sup>1</sup> The medical imaging research has shown that AT has the worst blood supply in the following range: if calcaneus is taken as an origin, the AT has a poor blood supply in its length between 2 and 6 cm, horizontally measured.<sup>2</sup> The AT is a key structure in the lower limb since it transmits force upward through the joint chain and further consumes energy through the bone and soft tissues. Farris et al.<sup>3</sup> found that the contribution of the AT to the ankle joint during running was more than 50%. Therefore, AT is related to the improvement of the running economy. Larger AT stiffness can significantly reduce oxygen

consumption, while longer AT arms can improve the running economy by reducing the required muscle activity.<sup>4</sup>

Concerning the load of the AT, at full speed run, the peak load of the AT is about 12.5 times the body

<sup>1</sup>Faculty of Sports Science, Ningbo University, Ningbo, China

<sup>2</sup>Doctoral School on Safety and Security Sciences, Obuda University, Budapest, Hungary

<sup>3</sup>Faculty of Engineering, University of Szeged, Szeged, Hungary

<sup>4</sup>Centre for Health and Exercise Science Research, Department of Sport, Physical Education and Health, Hong Kong Baptist University, Hong Kong, China

## Corresponding author:

Yaodong Gu, Faculty of Sports Science, Ningbo University, 818 Fenghua Road, Ningbo 315211, China.

Email: [guyaodong@nbu.edu.cn](mailto:guyaodong@nbu.edu.cn)

weight, during jumping or shuttle run, the peak load of the AT can reach 3–5 times the body weight.<sup>5</sup> AT is highly sensitive to mechanical stimuli, therefore regular exercise can increase the diameter of the AT, while less activity results in a decrease in the diameter.<sup>6</sup> The increase in elastic modulus and stiffness after training indicates that the AT will undergo adaptive changes after training to withstand higher stress.<sup>7</sup> Achilles tendon rupture (ATR) does not seem to affect neuromuscular control but may affect the output of the lower limb mechanical power during the stance period, thereby affecting joint stability.<sup>8</sup> Consequently, when discussing complex AT injuries, it is not possible to consider only the mechanical properties and functions of the AT itself.

The incidence of ATR continues to grow, the incidence on the left side is higher than on the right side while 75% of acute ATR is associated with exercise. Incidences regarded to the right side may be since the right leg is more often used to push the weight to the left leg.<sup>9</sup> The mechanism of injury can be related to rapid plantarflexion movements in the ankle joint when the soleus muscle contracts. This can be explained as follows: when stepping on the edge of the sidewalk, the knee is in full extension while at the same time the ankle joint is in full plantarflexion. At this moment a huge ankle dorsiflexion force is exerted on the foot likewise as an athlete jumps or falls from a height, then this dorsiflexion force can rupture the AT suddenly.<sup>10</sup> The ATR incidence is always at a high level in badminton sport, because of a large number of directional lunges, jumping, and landing movements.<sup>11</sup> Evidence has been reported that ATR will cause persistent tendon elongation and it is associated with biomechanical deficits such as decreased plantar flexor muscle strength/volume, decreased ankle joint proprioception, and reduced AT stiffness.<sup>12</sup>

The gait abnormalities and functional deficits have been found in the ruptured side compared with the contralateral side and healthy control group.<sup>13</sup> Experimental measures that quantify regional tendon strain are currently restricted to a small imaging region of a portion of the AT and less dynamic slow activities such as isolated contraction and walking.<sup>14</sup> Direct measurement of AT and foot internal tissue interactive forces and stresses are not ethically viable, therefore computational modeling, such as musculoskeletal modeling and finite element analysis are combined to investigate the relative effects of variations in tendon geometry and material properties on local stress and strain.<sup>15</sup> Therefore, the purpose of this study was to develop a computational methodology, which combines the subject-specific musculoskeletal model and finite element modeling to predict the foot internal stresses and strain based on medical imaging and gait analysis data. It was hypothesized that the injured AT would decrease the AT force (triceps surae muscle force) and redistribute the metatarsal strain and stresses during normal walking.

## Methods

### Participant

This study recruit one sub-elite badminton player (male, age: 27 years old, badminton experience: 16.5 years, BMI: 22.8 kg/m<sup>2</sup>) who sustained acute unilateral ATR 12 months ago. The percutaneous surgical repair was applied for the subject within 1 week of ATR injury. The rehabilitation program of the subject was made by a rehabilitation physiotherapist. The exclusion criteria were lower limb operation within 6 months, re-rupture of the injured AT or rupture of the contralateral AT.<sup>16</sup> Ethical approval was obtained by the local ethics committee in the University (No. RAGH202010160004) under the Declaration of Helsinki. The participant was informed of the experimental process and signed the informed consent before participation.

### Gait analysis

The lower extremity kinematics including hip, knee, ankle, and subtalar joints were recorded using an eight-camera high-speed motion capture system (VICON MX-T20, Oxford, UK, frequency = 200 Hz). The ground reaction forces were collected simultaneously using two 6 degrees of freedom force platforms (AMTI, Watertown, USA, frequency = 1000 Hz). In total 38 reflective skin markers were attached to the anatomic bony and digitized landmarks, as shown in Figure 1(a).<sup>17</sup> Participant was asked to walk barefoot at self-selected comfort speed over a 15 m walkway. Subjects were asked to hit the force platform with both feet respectively until 10 successful trials were obtained. The recorded lower limbs kinematics and kinetics were exported using the inherent Vicon Nexus 1.8.5 software, then the outputted .C3D files including joint kinematics and ground reaction forces (GRF) were collected as the input of musculoskeletal and finite element modeling.<sup>18</sup> The surface electromyography (EMG, Delsys, USA) signal of the bilateral triceps surae muscles (medial gastrocnemius, lateral gastrocnemius, and soleus) were taken at the frequency of 1000 Hz during each maximal voluntary isometric contraction (MVIC), bandpass filtered at 16 Hz–380 Hz, low-pass filtered at 7 Hz.<sup>19</sup> The kinematic and muscle activity data were represented as waveforms that changed continuously throughout the stance phase and were normalized into 101 data points.

### Musculoskeletal model

The generic Gait2392 musculoskeletal model upon adult cadaver data includes 12 rigid-body segments, 23 degrees of freedom, and 92 muscle-tendon actuators were used to determine lower extremity joint kinematics and optimize the bilateral triceps surae muscle forces, as shown in Figure 1(b).<sup>20</sup> The Clinical MR (magnetic resonance) images (Philips 3T, General Electric, USA)

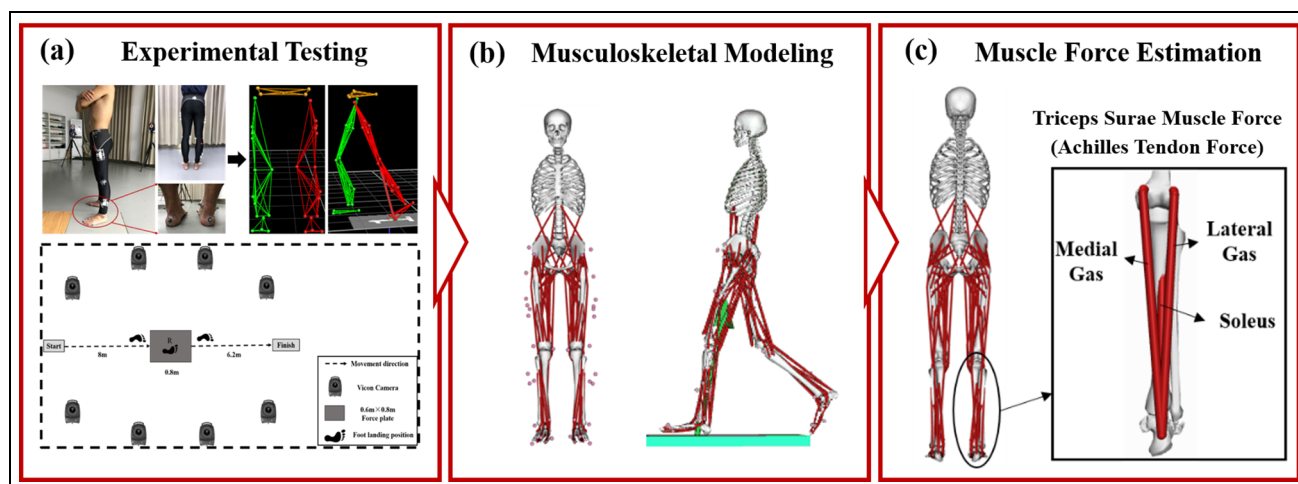


**Figure 1.** The workflow of experimental testing and musculoskeletal modeling.

scan the shank and the complete foot were performed when the subject laid in a prone position with their legs fully extended. The repetition time/echo time was set to 500/14ms, the field of view was 20cm and the slice thickness was 1mm. The segmentation was performed by the Mimics 20.0 software.<sup>21</sup> The insertion points of AT on the calcaneus as well as the AT slack length were determined from the reconstructed MR images.<sup>22</sup> The AT slack length and the triceps surae muscle optimal fiber length between the injured side and uninjured side was adjusted based on the measured MR images,<sup>23</sup> and further validated through ultrasound imaging system (Aloka, Tokyo, Japan) with the frequency of 10 MHz and a distance resolution of 0.26 mm.

Segment lengths, muscle attachment points, joint articulations, and muscle lengths were scaled to each participant based on anthropometric parameters and reflective markers attached to the body landmarks.<sup>24</sup> It should be noted that the use of altering the optimal fiber length and the tendon slack length in the patient-specific musculoskeletal model was a novel step for Achille tendon rupture musculoskeletal model building.<sup>25</sup> The Inverse Kinematics (IK) tool embedded in OpenSim minimizes the errors between experimentally tested marker trajectories and markers fixed to the model, which was used to determine the lower limb joint angles during each walking trial. The Inverse Dynamics (ID) tool was used to compute the external joint moments and determine the generalized forces at each joint. The workflow of the triceps surae muscle forces estimation was shown in Figure 1. The Static Optimization (SO) algorithm was used to calculate the muscle forces based on the three-element Hill-type muscle model, which minimizes the sum of muscle activations squared.<sup>26</sup> The gastrocnemius muscle weighting constant was set at 1.5, the hamstrings was set at 2, and 1 for the other muscles.<sup>27</sup> The triceps surae muscle forces were computed as the sum of medial

gastrocnemius force, lateral gastrocnemius force, and soleus force, which was considered as the AT force and normalized with body weight (BW).

### Finite element model

The DICOM format medical imaging files were imported into Mimics 18.0 (Materialize, Leuven, Belgium), and the image gray threshold segmentation method was used to determine the skeleton and soft tissue boundaries. The obtained STL file was imported into Geomagic Studio 12.0 (Geomagic, Inc., USA) for smoothing all the uneven surface, and then processed using Solidworks 2020 (SolidWorks Corporation, MA, United States) to generate a solid model of 28 bones including tibia, fibula, and foot bones and soft tissue.<sup>28</sup> In the finite element analysis software ANSYS Workbench 18.0, the mesh is divided and the model is established. The mesh type selects regular tetrahedral elements. The established three-dimensional finite element model of the foot and ankle include 28 bones, 72 ligaments, plantar fascia, and encapsulated soft tissue.<sup>29</sup> To simplify the complexity of the model, all bone, ligament, and cartilage materials in the model are idealized as uniform and isotropic elastic materials.<sup>30</sup> The contact behavior is defined between the articular surfaces of each group of bones, and the cartilage thickness is set according to known literature reports. The material properties and unit types of various organizations are shown in Table 1.<sup>31</sup>

Ligaments and plantar fascia were regarded as materials that bear tensile loads without being compressed, and the external soft tissues were defined as elastic materials. The ankle ligaments and plantar fascia were connected by truss elements. The AT was attached to the calcaneal tubercle, which allows the MG, LG, and SOL muscle forces to apply a uniformly distributed AT tension throughout the whole AT cross-sectional area.<sup>32</sup>

**Table 1.** Material properties and element types of the finite element model.

Component	Element type	Elasticity modulus E (MPa)	Poisson's ratio	Cross-section area (mm <sup>2</sup> )
Bone	Tetrahedron	29200	0.30	—
Cartilage	Tetrahedron	1	0.40	—
Ligament	Truss	260	—	18.4
Plantar fascia	Truss	350	—	58.6
Soft tissue	Tetrahedron	0.15	0.45	—

A three-dimensional soft tissue was reconstructed to encapsulate all the tendons, ligaments, and foot musculoskeletal elements (see Figure 2).

To simulate the propulsion phase of the foot during walking, a non-deformable solid ground was established in the model and the material properties were assigned.<sup>33</sup> The contact behavior was established between the foot and the ground, the friction coefficient was set to 0.6, the loading and boundary conditions of the foot and ankle were shown in Figure 2.<sup>34</sup>

The previous research found that patients with unilateral ATR had bilateral lower extremity gait asymmetry during the rehabilitation period. The ankle and foot of the affected lower extremity showed an inversion tendency during walking. The calf muscle strength decreases on the injured side. Therefore, in this study, the individualized musculoskeletal model was first used to optimize the calculation of bilateral lower limb gastrocnemius and soleus muscle strength, and the algebraic sum of the two was used to express the combined force of the calf triceps. The stress distribution of the metatarsals during the gait propulsion phase was studied. The bodyweight of the selected represent subject is 68 kg, thus the vertical ground reaction force was set to 340 N (50% of body weight).<sup>35</sup> According to the principle of force equivalent interchangeability, a ground reaction force of 340 N was applied to the ground in a direction perpendicular to the support upward. After the boundary and loading conditions were settled, the finite element model of the foot and ankle was calculated during the propulsion phase, and the general statics algorithm was used in the ANSYS Workbench 18.0 software.<sup>36</sup> The von Mises stress of the five metatarsals was extracted.

### Model validation

**Musculoskeletal model validation.** For the musculoskeletal model validation, the estimated muscle activation extracted from OpenSim were compared with the recorded EMG during the stance phase for the subject qualitatively.<sup>37</sup> The recorded root mean square (RMS) of the medial and lateral gastrocnemius during the stance phase of walking were found similar and in good agreement with the predicted muscle activation. The calculated joint kinematics from the IK tool and the joint external moments from the Inverse Dynamics (ID)

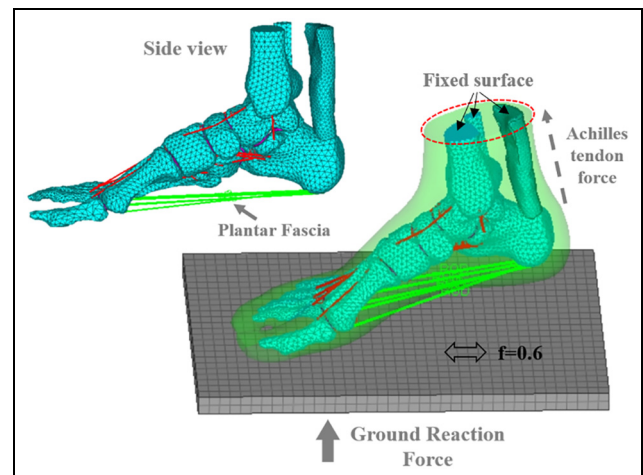


**Figure 2.** The three-dimensional finite element model of the foot and ankle complex.

tool were compared with previously published studies, the tendency and amplitude were found approaching one another.<sup>38</sup> Thus, the obtained triceps surae muscle force was used to define the muscle loading condition for the finite element foot simulation.

**Finite element model validation.** The plantar pressure plate (Novel, Munich, Germany) was used to measure the plantar pressure of the patient, and then the collected plantar pressure distribution was compared with the predicted plantar pressure by the finite element analysis, and the peak values were compared to verify the validity of the model.<sup>39</sup> With the loading of 340 N ground reaction force to simulate the natural standing of both feet, the plantar pressure distribution trend of the model established in this study was similar compared with previous studies. It is verified that the peak pressure of the finite element simulation is 0.36 MPa, the peak value of the plantar pressure test result is 0.17 MPa, and the peak plantar pressure appears in the heel area. In this study, when the finite element simulation under the condition of 340 N ground reaction force, the peak plantar pressure was 0.18 MPa, the peak value was also distributed under the heel region.<sup>15</sup> In summary, the three-dimensional foot-ankle complex finite element model established in this study was effective.

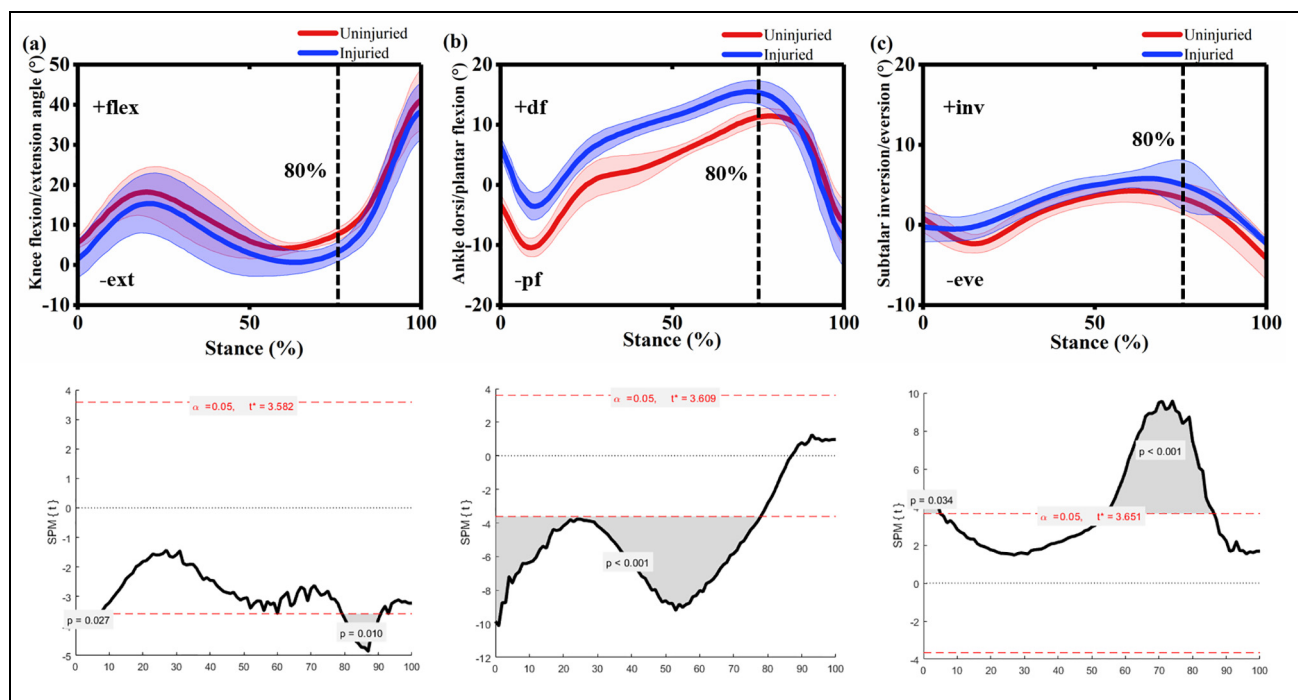


**Figure 3.** The calculated knee joint flexion/extension, ankle joint dorsiflexion/plantarflexion and subtalar joint inversion/eversion (a–c) during the stance phase (100%) of walking for the injured side (blue) and the uninjured side (red).

### Statistical analysis

The stance phase of the bilateral lower limbs during walking from heel strike to toe-off was selected and analyzed in this study. The knee flexion/extension, ankle dorsiflexion/plantarflexion, and subtalar inversion/eversion angle, the medial gastrocnemius, lateral gastrocnemius, and soleus muscle forces raw data from 10 trials of each subject were interpolated into 101 data points to represent the stance phase. The muscle forces were normalized to body weight (BW). The 1D Statistical parametric mapping (SPM) paired-sample t-test was performed to compare the joint kinematics and muscle forces between uninjured and injured sides, due to the one-dimensional time-series characteristics.<sup>40</sup> All statistical analyses were performed in Matlab R2018a (MathWorks Inc., Natick, MA, USA), the significance level was set at 0.05.

## Results

### Lower extremity kinematics

The subject walked with a velocity of 1.42 m/s, a stride length of 1.49 m. The knee and ankle joints sagittal plane and the subtalar joint frontal plane kinematics were extracted for the SPM1D analyses. At the knee joint during the stance phase of walking, the knee flexion angle decreased in the injured side at 0%–3% ( $p = 0.027$ ), and 63%–80% ( $p = 0.010$ ), as shown in Figure 3(a). At the ankle joint during the stance phase of walking, the ankle plantarflexion angle decreased in

the injured side at 0%–78% ( $p < 0.001$ ), as shown in Figure 3(b). At the subtalar joint in the frontal plane, the inversion angle increased in the injured side at 0%–4% ( $p = 0.034$ ), and 56%–87% ( $p < 0.001$ ), as shown in Figure 3(c). At 80% time point during the push-off phase, the ankle plantarflexion angle decreased by 39.6% on the injured side, the subtalar inversion angle increased by 22.9% in the injured side compared with the uninjured side, respectively.

### AT length and force

The injured AT slack length was found elongated compared with the uninjured side, and the average percentage was 5.5%. The triceps surae muscles including the medial gastrocnemius, lateral gastrocnemius, and soleus forces during the stance phase of walking were estimated and recorded to represent the AT force, as shown in Figure 4. The medial gastrocnemius muscle force decreased at 7%–12% ( $p = 0.006$ ), 20%–46% ( $p < .001$ ), and 68%–86% ( $p < 0.001$ ) in the injured side compared with the uninjured, as shown in Figure 4(a). The lateral gastrocnemius muscle force decreased at 3%–44% ( $p < 0.001$ ), 68%–87% ( $p < 0.001$ ), 97%–98% ( $p = 0.049$ ) in the injured side, as shown in Figure 4(b). The soleus muscle force decreased in the injured side at 69%–95% ( $p < 0.001$ ), as shown in Figure 4(c). At 80% time point during the push-off phase, the AT force was decreased by 21.9% in the injured side compared with the uninjured side.



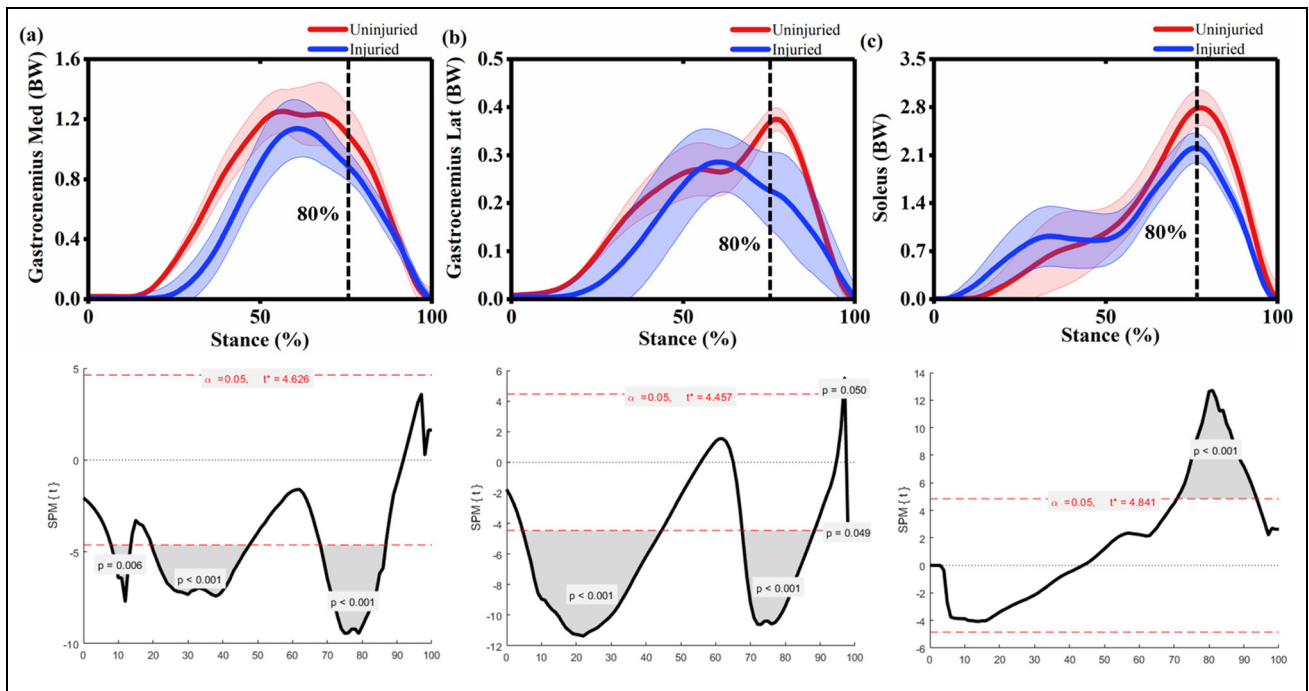


**Figure 4.** The estimated gastrocnemius medialis (a), gastrocnemius lateralis (b) and soleus(c) forces during the stance phase (100%) of walking for the injured side (blue) and the uninjured side (red).

### Stress distribution on the metatarsals

The finite element simulation at the late stance phase was performed to observe the metatarsals stresses. The foot in the injured side was more inverted, and the plantarflexion degree was declined during the late stance compared with the uninjured side. The triceps surae muscle force namely the AT force was decreased in the injured side during the late stance of walking. The von Mises stress in the five metatarsals was redistributed due to AT injury, as shown in Figure 5. Compared to the uninjured side, the lateral forefoot suffered from higher von Mises stress on the injured side. The AT injured foot showed significant increases in von Mises stress at the fourth (9.86 MPa for the injured while 3.99 MPa for the uninjured, 59.5%) and fifth (5.66 MPa for the injured while 0.80 MPa for the uninjured, 85.9%) metatarsals, and decrease at the first (0.41 MPa for the injured while 4.90 MPa for the uninjured, 91.6%) and second (1.94 MPa for the injured while 5.88 MPa for the uninjured, 67.0%) metatarsals, as shown in Figure 5.

### Discussion

The finite element foot model constructed in this study assists the experimental gait analysis to assess the foot internal complex biomechanical behavior and calculate the unmeasurable metatarsal stress. The subject-specific foot-ankle geometry, as well as the AT morphology, were reconstructed through medical images. Three-dimensional foot and ankle kinematics and vertical

ground reaction forces were measured in a gait analysis laboratory to define the boundary conditions in the finite element model. The subject-specific musculoskeletal model was applied to obtain the individualized muscle forces loading conditions between the injured side and uninjured side. Most of the previous studies quote the muscle force from the literature, or muscle electromyography signal, or the muscle force linearly proportional to physiological cross-sectional area (PCSA) assumption, or reverse predicted by the using of joint moments.<sup>34,41,42</sup> The calculated muscle forces using static optimization (SO) tool as input could improve the predictive accuracy of metatarsal stress from the finite element model.<sup>15</sup>

The AT elongation was found in the injured side after 12 months of surgical repair compared with the uninjured side (5.5%). Thus, the tendon slack length and optimal muscle fiber length of the three ankle plantar flexor muscles medial gastrocnemius, lateral gastrocnemius, and soleus muscles between the two sides were modified proportionally in OpenSim.<sup>43</sup> The subject-specific musculoskeletal model may increase the prediction accuracy of muscle forces. The foot-ankle complex finite element model contains most of the musculoskeletal components, which include 28 bony structures, reconstructed AT, cartilage layers, plantar fascia, ligament bundles, and 3D encapsulated soft tissues. The tetrahedral elements mesh was applied for bony, cartilage, and encapsulated soft tissue instead of hexahedral elements, which was due to the similar accuracy and ability for the calculation of peak von Mises stress, except that the use of tetrahedral elements may increase

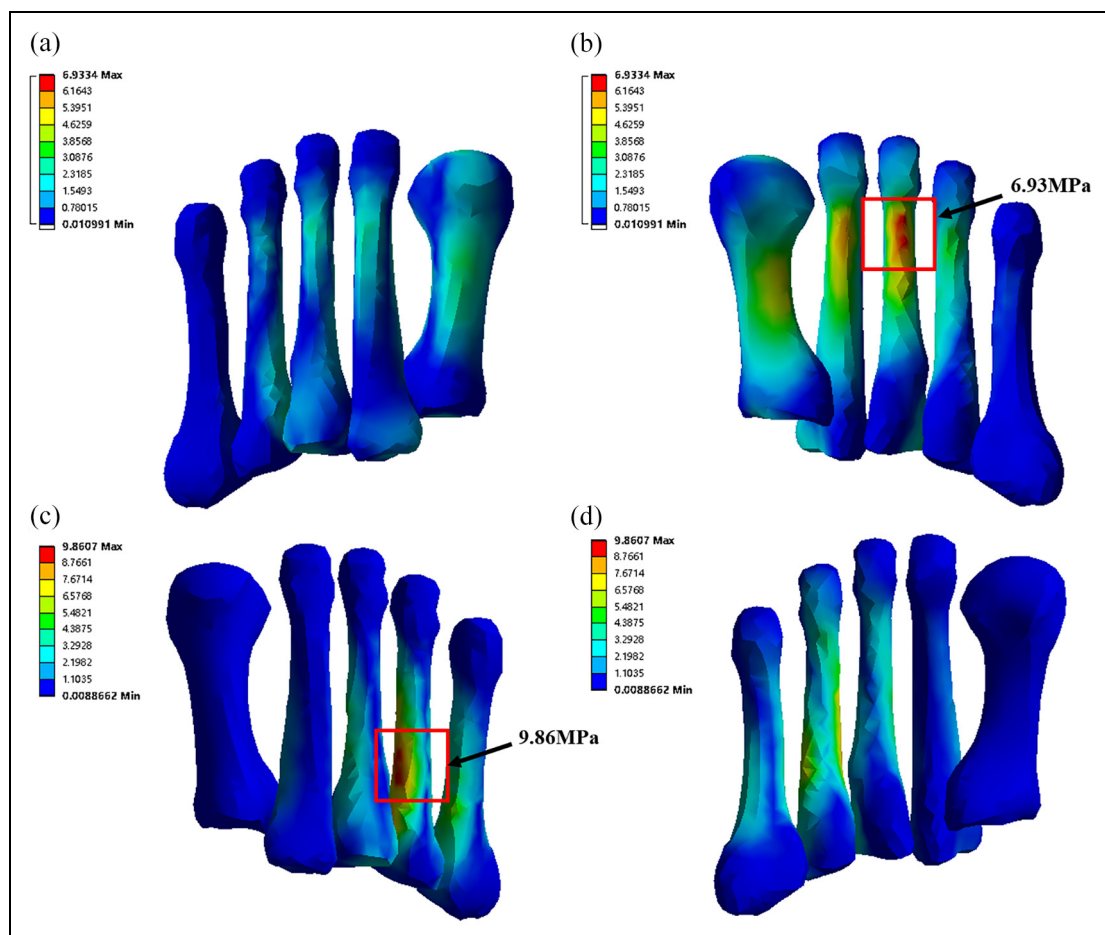


**Figure 5.** The comparison of von Mises stress at the five metatarsals between the injured and uninjured sides (A&B front and back view of metatarsals in the uninjured side; C&D front and back view of metatarsals in the injured side).

computer calculation time.<sup>44</sup> The material properties of the above-mentioned components were defined as consistent between the injured and uninjured sides. The sensitivity of the finite element model was verified by comparing the tested plantar pressure and predicting specific region peak and average plantar pressure during balanced barefoot standing.<sup>45</sup> The compared plantar pressure was found in good agreement between the predicted and tested results, the average and peak pressure percent errors were lower than 10%. To understand the influence of unilateral ATR on foot internal biomechanics asymmetry, and further improve the effectiveness of rehabilitation and treatment.<sup>46</sup> A combined subject-specific musculoskeletal and foot-ankle complex finite element model was developed to provide potential information for the study purposes and clinical application.<sup>47</sup>

The late stance phase of walking (60%–100%) was selected for the finite element analysis, the 60% of the stance phase was defined as initial push-off and the heel start to arise. The 80% moment during the push-off phase was selected as the target point for finite element analysis.<sup>48</sup> The reason was that in this special moment, the ankle plantarflexion, subtalar inversion, and AT force were almost in their peak values. The ankle joint

dorsiflexion transit to plantarflexion, and the AT force increase rapidly to lift the heel during the push-off phase.<sup>49</sup> The main asymmetry appears at the 80% moment of stance phase between the injured side and uninjured side were found as below: (1) The ankle plantarflexion angle in the injured side was significantly decreased by 39.6% compared to the uninjured side; (2) The subtalar joint inversion angle degree, also known as the foot was found more inverted (22.9%) in the injured side; (3) The triceps surae muscle atrophy was observed obviously in the ATR side (21.9%). As expected, along with the different boundary and loading conditions given to the injured and uninjured foot-ankle finite element model, the metatarsals stresses were redistributed in the push-off phase, which was also in agreement with previous studies.<sup>42,50,51</sup> The von Mises stress on the fourth and fifth metatarsals was increased by 59.5% and 85.9% on the injured side. While the normal side showed the concentration under the second and third metatarsals.

The increased peak von Mises stress of the fourth and fifth metatarsals indicates that the ATR side may undergo higher injury risks of the fourth and fifth metatarsals.<sup>52</sup> The elongated AT and altered mechanical properties after rupture may affect the force

transmission from the triceps surae muscle.<sup>53</sup> Which accompanied by decreased ankle plantar flexor strength may responsible for the descend control ability of the foot in the frontal plane.<sup>54</sup> Therefore, the ankle-foot lateral sprain injury risk will be aggrandized in the AT injured side.<sup>55</sup> The physical activity level and major functional deficits were observed to persist even 2–6 years after tendon rupture.<sup>56</sup> Previous research also found that the soleus tendon and gastrocnemius tendon were significantly elongated in the ruptured side, which was accompanied by decreased fascicle length of the gastrocnemius muscle and persistent functional deficits.<sup>53</sup> The AT anatomical changes and the appearance of triceps surae muscle weakness may be caused by the decreased force transmission capability of the tendon.<sup>57</sup> The ankle plantar flexors were operated primarily in the sagittal plane, while the increased loading in the frontal plane may compensate for the deficit in the sagittal plane.<sup>58</sup> Thus, the foot and ankle inversion degree increased in the injured side, and corresponding with higher metatarsal stresses distribute on the lateral plantar. Decreased knee flexion angle was found decreased in the injured, which may weaken the cushion effect of the lower extremity.<sup>59</sup> A recent study found that patients after an ATR suffer from higher knee abduction moments and knee joint loading in the ruptured side.<sup>60</sup>

Several limitations should not be ignored in this study, the first limitation was the cross-sectional design of the experiment. Thus, the biomechanical and functional variations were not clear as causes or consequences after an ATR. A long-term follow-up study design may provide more information for a better understanding of the injury mechanism of ATR. Secondly, only the barefoot condition was included in this study, while the comparison of barefoot and shod walking was not considered. Thirdly, the ATR mostly occurs during plantar flexors suffering rapid eccentric loading. Therefore, future studies should include cutting, landing, stop and go movements, which investigate the limb alignment and explosive actions after the ATR.<sup>13</sup> Moreover, the muscle force estimation was relied on the static optimization algorithm, while the recorded muscle activation data through surface EMG were not accounted, thus the Computed Muscle Control (CMC) method should be considered in the future.<sup>61</sup> The AT material property was taken from the previous study, and the foot-ankle complex geometry was obtained in an unloaded position from the MRI scanning. Thus, the finite element model sensitivity should be performed in future studies. Future research should consider follow-up study design and include movements suffering rapid eccentric loading.

## Conclusions

In this study, a computational methodology that combines the subject-specific musculoskeletal model and

finite element modeling was developed to predict the foot internal stresses and strain based on medical imaging and gait analysis data. It was found that an ATR influences the ipsilateral foot metatarsal stress distribution during walking compared to the uninjured side. Higher stress on the fourth and fifth metatarsals may increase the risk of stress-related and ankle lateral sprain injuries. Future studies should consider follow-up experimental design and include maneuvers like landing, cutting, and hopping.


## Declaration of conflicting interests

The author(s) declared no potential conflicts of interest with respect to the research, authorship, and/or publication of this article.

## Funding

The author(s) disclosed receipt of the following financial support for the research, authorship, and/or publication of this article: This study was sponsored by the Key R&D Program of Zhejiang Province China (2021C03130), Zhejiang Province Science Fund for Distinguished Young Scholars (LR22A020002), Public Welfare Science and Technology Project of Ningbo, China (No. 2021S134), The teaching and research project of Ningbo University (No. JYXMXZD2022008), Badminton World Federation (BWF) Sports Science project, and K.C. Wong Magna Fund in Ningbo University.

## ORCID iD

Yaodong Gu  <https://orcid.org/0000-0003-2187-9440>

## References

1. Saini SS, Reb CW, Chapter M, et al. Achilles tendon disorders. *J Am Osteopath Assoc* 2015; 115: 670–676.
2. Galanty HL and Bradley JP. Achilles tendon ruptures. *Top Emerg Med* 1995; 17: 36–46.
3. Farris DJ, Buckeridge E, Trewartha G, et al. The effects of orthotic heel lifts on achilles tendon force and strain during running. *J Appl Biomech* 2012; 28: 511–519.
4. Werkhausen A, Cronin NJ, Albracht K, et al. Training-induced increase in Achilles tendon stiffness affects tendon strain pattern during running. *PeerJ* 2019; 7: e6764.
5. Baxter JR, Corrigan P, Hullfish TJ, et al. Exercise progression to incrementally load the achilles tendon. *Med Sci Sports Exerc* 2021; 53: 124–130.
6. Obst SJ, Barrett RS and Newsham-West R. Immediate effect of exercise on Achilles tendon properties: systematic review. *Med Sci Sports Exerc* 2013; 45: 1534–1544.
7. Pizzolato C, Shim VB, Lloyd DG, et al. Targeted Achilles tendon training and rehabilitation using personalized and real-time multiscale models of the neuromusculoskeletal system. *Front Bioeng Biotechnol* 2020; 8: 878.
8. Patrick MW, Jan PH, Harlow E, et al. Tendon lengthening after achilles tendon rupture—passive effects on the ankle joint in a cadaveric pilot study simulating weight bearing. *Injury* 2020; 51: 532–536.



9. Lantto I, Heikkinen J, Flinkkilä T, et al. Epidemiology of Achilles tendon ruptures: increasing incidence over a 33-year period. *Scand J Med Sci Sport* 2015; 25: e133–e138.
10. Tarantino D, Palermi S, Sirico F, et al. Achilles tendon rupture: mechanisms of injury, principles of rehabilitation and return to play. *J Funct Morphol Kinesiol* 2020; 5: 95.
11. Bravo-Sánchez A, Abián P, Jimenez F, et al. Structural and mechanical properties of the Achilles tendon in senior badminton players: operated vs. non-injured tendons. *Clin Biomech* 2021; 85: 105366.
12. Diniz P, Pacheco J, Guerra-Pinto F, et al. Achilles tendon elongation after acute rupture: is it a problem? a systematic review. *Knee Surg Sport Tr A* 2020; 28: 4011–4030.
13. Speedtsberg MB, Kastoft R, Barfod KW, et al. Gait function and postural control 4.5 years after nonoperative dynamic treatment of acute Achilles tendon ruptures. *Orthop J Sport Med* 2019; 7: 2325967119854324.
14. Handsfield GG, Greiner J, Madl J, et al. Achilles subtenon structure and behavior as evidenced from tendon imaging and computational modeling. *Front Sport Act Living* 2020; 2: 70.
15. Scarton A, Guiotto A, Malaquias T, et al. A methodological framework for detecting ulcers' risk in diabetic foot subjects by combining gait analysis, a new musculoskeletal foot model and a foot finite element model. *Gait Posture* 2018; 60: 279–285.
16. Meulenkamp B, Stacey D, Fergusson D, et al. Protocol for treatment of Achilles tendon ruptures: a systematic review with network meta-analysis. *Syst Rev* 2018; 7: 1–7.
17. Sharpe T, Malone A, French H, et al. Effect of flip-flops on lower limb kinematics during walking: a cross-sectional study using three-dimensional gait analysis. *Ir J Med Sci* 2016; 185: 493–501.
18. Halonen KS, Dzialo CM, Mannisi M, et al. Workflow assessing the effect of gait alterations on stresses in the medial tibial cartilage – combined musculoskeletal modelling and finite element analysis. *Sci Rep* 2017; 7: 17396.
19. Papagiannis GI, Triantafyllou AI, Roumpelakis IM, et al. Methodology of surface electromyography in gait analysis: review of the literature. *J Med Eng Technol* 2019; 43: 59–65.
20. Mei Q, Gu Y, Xiang L, et al. Foot pronation contributes to altered lower extremity loading after long distance running. *Front Physiol* 2019; 10: 573.
21. Li S, Zhang Y, Gu Y, et al. Stress distribution of metatarsals during forefoot strike versus rearfoot strike: a finite element study. *Comput Biol Med* 2017; 91: 38–46.
22. Hansen W, Shim VB, Obst S, et al. Achilles tendon stress is more sensitive to subject-specific geometry than subject-specific material properties: a finite element analysis. *J Biomech* 2017; 56: 26–31.
23. Sun D, Fekete G, Mei Q, et al. Gait abnormality and asymmetry analysis after 18–24 months surgical repair of unilateral Achilles tendon rupture. *J Med Imaging Heal Informatics* 2019; 9: 552–560.
24. Hicks JL, Uchida TK, Seth A, et al. Is my model good enough? best practices for verification and validation of musculoskeletal models and simulations of movement. *J Biomech Eng* 2015; 137: 020905.
25. Smale KB, Conconi M, Sancisi N, et al. Effect of implementing magnetic resonance imaging for patient-specific OpenSim models on lower-body kinematics and knee ligament lengths. *J Biomech* 2019; 83: 9–15.
26. Sritharan P, Perraton LG, Munoz MA, et al. Muscular coordination of single-leg hop landing in uninjured and anterior cruciate ligament-reconstructed individuals. *J Appl Biomech* 2020; 36: 235–243.
27. Lerner ZF, DeMers MS, Delp SL, et al. How tibiofemoral alignment and contact locations affect predictions of medial and lateral tibiofemoral contact forces. *J Biomech* 2015; 48: 644–650.
28. Zhang Y, Awrejcewicz J, Szymanowska O, et al. Effects of severe hallux valgus on metatarsal stress and the metatarsophalangeal loading during balanced standing: a finite element analysis. *Comput Biol Med* 2018; 97: 1–7.
29. Morales-Orcajo E, Souza TR, Bayod J, et al. Non-linear finite element model to assess the effect of tendon forces on the foot-ankle complex. *Med Eng Phys* 2017; 49: 71–78.
30. Li Y, Leong KF and Gu Y. Construction and finite element analysis of a coupled finite element model of foot and barefoot running footwear. *Proc Inst Mech Eng Part P J Sport Eng Technol* 2019; 233: 101–109.
31. Peng Y, Wong DW-C, Chen TL-W, et al. Influence of arch support heights on the internal foot mechanics of flatfoot during walking: a muscle-driven finite element analysis. *Comput Biol Med* 2021; 132: 104355.
32. Morales-Orcajo E, Bayod J and de Las Casas EB. Computational foot modeling: scope and applications. *Arch Comput Methods Eng* 2016; 23: 389–416.
33. Taha Z, Norman MS, Omar SFS, et al. A finite element analysis of a human foot model to simulate neutral standing on ground. *Proc Eng* 2016; 147: 240–245.
34. Akrami M, Qian Z, Zou Z, et al. Subject-specific finite element modelling of the human foot complex during walking: sensitivity analysis of material properties, boundary and loading conditions. *Biomech Model Mechanobiol* 2018; 17: 559–576.
35. Isvilanonda V, Dengler E, Iaquinto JM, et al. Finite element analysis of the foot: model validation and comparison between two common treatments of the clawed hallux deformity. *Clin Biomech* 2012; 27: 837–844.
36. Chen TLW, Wong DWC, Wang Y, et al. Foot arch deformation and plantar fascia loading during running with rearfoot strike and forefoot strike: a dynamic finite element analysis. *J Biomech* 2019; 83: 260–272.
37. Alvim FC, Lucareli PRG and Menegaldo LL. Predicting muscle forces during the propulsion phase of single leg triple hop test. *Gait Posture* 2018; 59: 298–303.
38. Raabe ME and Chaudhari AMW. An investigation of jogging biomechanics using the full-body lumbar spine model: model development and validation. *J Biomech* 2016; 49: 1238–1243.
39. Ielapi A, Lammens N, Van Paepegem W, et al. A validated computational framework to evaluate the stiffness of 3D printed ankle foot orthoses. *Comput Methods Biomech Biomed Engin* 2019; 22: 880–887.
40. Honert EC and Pataky TC. Timing of gait events affects whole trajectory analyses: a statistical parametric mapping sensitivity analysis of lower limb biomechanics. *J Biomech* 2021; 119: 15.
41. Johnson S and Ou H. Effects of boundary conditions on foot behaviour in the standing position in 3D finite element foot model. *J Foot Ankle Res* 2014; 7: 1–2.
42. Wang Y, Li Z, Wong DWC, et al. Finite element analysis of biomechanical effects of total ankle arthroplasty on the foot. *J Orthop Transl* 2018; 12: 55–65.

43. Aufwerber S, Edman G, Grävare Silbernagel K, et al. Changes in tendon elongation and muscle atrophy over time after achilles tendon rupture repair: a prospective cohort study on the effects of early functional mobilization. *Am J Sports Med* 2020; 48: 3296–3305.
44. Chen WM, Cai YH, Yu Y, et al. Optimal mesh criteria in finite element modeling of human foot: The dependence for multiple model outputs on mesh density and loading boundary conditions. *J Mech Med Biol* 2021; 21: 2140034.
45. Omasta M, Paloušek D, Návrát T, et al. Finite element analysis for the evaluation of the structural behaviour, of a prosthesis for trans-tibial amputees. *Med Eng Phys* 2012; 34: 38–45.
46. Pope JP, Pelletier LG and Guertin C. Examining the role ones' stage of change plays in understanding the relationship between motivation and physical activity. *Phys Act Heal* 2021; 5: 120–132.
47. Sun D, Fekete G, Baker JS, et al. A pilot study of musculoskeletal abnormalities in patients in recovery from a unilateral rupture-repaired achilles tendon. *Int J Environ Res Public Health* 2020; 17: 4642.
48. Wong DWC, Wang Y, Chen TLW, et al. Finite element analysis of generalized ligament laxity on the deterioration of hallux valgus deformity (Bunion). *Front Bioeng Biotechnol* 2020; 8: 1062.
49. Guilleron C, Durand S, Maktouf W, et al. Rearfoot-forefoot profile defined by vertical ground reaction forces during gait is altered in patients with unilateral intermittent claudication. *J Biomech* 2020; 109: 109966.
50. Gu YD, Ren XJ, Li JS, et al. Computer simulation of stress distribution in the metatarsals at different inversion landing angles using the finite element method. *Int Orthop* 2010; 34: 669–676.
51. Firminger CR, Fung A, Loundagin LL, et al. Effects of footwear and stride length on metatarsal strains and failure in running. *Clin Biomech* 2017; 49: 8–15.
52. Fung A, Loundagin LL and Edwards WB. Experimental validation of finite element predicted bone strain in the human metatarsal. *J Biomech* 2017; 60: 22–29.
53. Suydam SM, Buchanan TS, Manal K, et al. Compensatory muscle activation caused by tendon lengthening post-Achilles tendon rupture. *Knee Surg Sport Tr A* 2015; 23: 868–874.
54. Silbernagel KG, Steele R and Manal K. Deficits in heel-rise height and Achilles tendon elongation occur in patients recovering from an Achilles tendon rupture. *Am J Sports Med* 2012; 40: 1564–1571.
55. Jandacka D, Silvernail JF, Uchytel J, et al. Do athletes alter their running mechanics after an Achilles tendon rupture? *J Foot Ankle Res* 2017; 10: 1–8.
56. Agres AN, Duda GN, Gehlen TJ, et al. Increased unilateral tendon stiffness and its effect on gait 2-6 years after Achilles tendon rupture. *Scand J Med Sci Sport* 2015; 25: 860–867.
57. Ahmed HM and Babakir-Mina M. Population-level interventions based on walking and cycling as a means to increase physical activity. *Phys Act Heal* 2021; 5: 55–63.
58. Tengman T and Riad J. Three-dimensional gait analysis following achilles tendon rupture with nonsurgical treatment reveals long-term deficiencies in muscle strength and function. *Orthop J Sport Med* 2013; 1: 2325967113504734.
59. Agopyan H, Griffet J, Poirier T, et al. Modification of knee flexion during walking with use of a real-time personalized avatar. *Heliyon* 2019; 5: e02797.
60. Jandacka D, Plesek J, Skypala J, et al. Knee joint kinematics and kinetics during walking and running after surgical Achilles tendon repair. *Orthop J Sport Med* 2018; 6: 2325967118779862.
61. Karimi MT, Hemmati F, Mardani MA, et al. Determination of the correlation between muscle forces obtained from OpenSim and muscle activities obtained from electromyography in the elderly. *Phys Eng Sci Med* 2021; 44: 243–251.